

Quantum chemistry on quantum annealers

Scott N. Genin

OTI Lumionics Inc., 100 College St. #351, Toronto, Ontario M5G 1L5, Canada

Ilya G. Ryabinkin*

OTI Lumionics Inc., 100 College St. #351, Toronto, Ontario M5G 1L5, Canada

Department of Physical and Environmental Sciences,

University of Toronto Scarborough, Toronto, Ontario M1C 1A4, Canada and

Chemical Physics Theory Group, Department of Chemistry,

University of Toronto, Toronto, Ontario M5S 3H6, Canada

Artur F. Izmaylov

Department of Physical and Environmental Sciences,

University of Toronto Scarborough, Toronto, Ontario M1C 1A4, Canada and

Chemical Physics Theory Group, Department of Chemistry,

University of Toronto, Toronto, Ontario M5S 3H6, Canada

(Dated: January 16, 2019)

Quantum chemistry calculations for small molecules on quantum hardware have been demonstrated to date only on universal-gate quantum computers, not quantum annealers. The latter devices are limited to finding the lowest eigenstate of the Ising Hamiltonian whereas the electronic Hamiltonian could not be mapped to the Ising form without exponential growth of the Ising Hamiltonian with the size of the system [J. Phys. Chem. B **122**, 3384 (2018)]. Here we propose a novel mixed *discrete-continuous* optimization algorithm, which finds the lowest eigenstate of the qubit coupled cluster (QCC) method using a quantum annealer for solving a discrete part of the problem. The QCC method is a potentially exact approach for constructing the electronic wavefunction in the qubit space. Therefore, our methodology allows for systematically improvable quantum chemistry calculations using quantum annealers. We illustrate capabilities of our approach by calculating QCC ground electronic states for the LiH, H₂O, and C₆H₆ molecules. C₆H₆ calculations involve 36 qubits and are the largest quantum chemistry calculations made on a quantum annealer (the D-Wave 2000Q system) to date. Our findings opens up a new perspective for use quantum annealers in high-throughput material discovery.

I. INTRODUCTION

Quantum chemistry simulations are often considered as an ideal application of quantum computers following inspiring ideas of R. Feynman.¹ This tacitly assumes that the quantum computer is the universal one, capable of simulating quantum evolution governed by an arbitrary Hamiltonian. However, fundamental and technological obstacles with building such a universal quantum device prompted researchers and engineers to consider more limited architectures, such as quantum annealers. Quantum annealers,²⁻⁴ also known as Ising machines,⁵⁻⁷ can only find the ground state of the Ising Hamiltonian,⁸

$$\hat{H}_{\text{Is}} = \sum_{i=1}^N h_i \hat{z}_i + \sum_{i,j=1}^N J_{ij} \hat{z}_i \hat{z}_j, \quad (1)$$

where \hat{z}_i is the Pauli z -operator acting on the i -th spin (qubit), h_i and J_{ij} are constants that can be tuned independently.²

Since the molecular Hamiltonian is not in the Ising form, the electronic structure problem cannot be set up and solved directly on quantum annealers. However, there is still a strong impetus for use annealers due to their intrinsic ability to solve hard optimization problems⁹ (but also see a counterexample, Ref. 10). To date, only one

work¹¹ proposed a mapping of a general qubit Hamiltonian to the Ising form. Unfortunately, the qubit size of the resulting Ising Hamiltonian grows exponentially with the size of the system making this approach viable only for small systems (*e.g.* H₂ and LiH). Moreover, to reach chemical accuracy (≤ 1 kcal mol⁻¹) for H₂ in the minimal STO-3G basis required ~ 1400 qubits on the D-Wave 2000Q system.¹²

Here we take a different route. Instead of trying to use quantum annealing for the whole problem, we employ it as a part of a hybrid quantum-classical scheme that accelerates the convergence in the qubit coupled cluster (QCC) method.¹³ This method has been originally introduced for solving the electronic structure problem on a universal quantum computer within the variational quantum eigensolver (VQE) framework.^{14,15} Here, we do not employ a universal quantum computer but instead use the QCC energy functional for establishing the variational optimization problem. Even though this optimization problem is nonlinear, certain symmetries of the QCC energy functional allows us to substantially reduce the domain of continuous optimization variables by introducing auxiliary discrete variables. Discrete optimization is usually an exponentially difficult problem requiring combinatorial search, and it may seem that such a reduction of the domain only makes the problem harder. However,

in this case, it is possible to perform the discrete optimization by finding the lowest eigenstate of some Ising Hamiltonian. Therefore, a quantum annealer becomes essential in reducing the complexity of the QCC nonlinear optimization by solving the discrete part of the problem.

The rest of the paper is organized as follows. After a brief review of the electronic structure problem and the QCC method we show how the domain reduction idea can be integrated into the QCC framework. In particular, we discuss how the discrete optimization can be introduced in the QCC formalism, and how the Ising Hamiltonian whose lowest eigenstate is the solution for the discrete problem can be formulated. We illustrate our developments by solving the electronic structure problem for LiH, H₂O, and C₆H₆ molecules on a simulated perfect quantum annealer and the D-Wave 2000Q system.¹⁶

II. THEORY

A. Electronic structure problem

Electronic structure calculations amount to finding the solution of the time-independent electronic Schrödinger equation,

$$\hat{H}_e \Psi_i(\bar{\mathbf{r}}|\bar{\mathbf{R}}) = E_i(\bar{\mathbf{R}}) \Psi_i(\bar{\mathbf{r}}|\bar{\mathbf{R}}). \quad (2)$$

Here \hat{H}_e is the electronic Hamiltonian of a molecule with electronic variables $\bar{\mathbf{r}} = (\mathbf{r}_1, \dots, \mathbf{r}_{N_e})$ and nuclear configuration parameters $\bar{\mathbf{R}} = (\mathbf{R}_1, \dots, \mathbf{R}_N)$. $E_i(\bar{\mathbf{R}})$ and $\Psi_i(\bar{\mathbf{r}}|\bar{\mathbf{R}})$ are potential energy surfaces (PESs) and electronic wave functions, respectively. Eq. (2) is a many-body fermionic problem that defines electronic properties of molecules and materials from first principles, *i.e.* solely from knowledge of type and location of nuclei and the number of electrons N_e .

For transforming Eq. (2) to a qubit form, the differential operator \hat{H}_e is considered as an operator in a finite-dimensional Fock space using the second quantization formalism:

$$\hat{H}_e = \sum_{ij} h_{ij} \hat{a}_i^\dagger \hat{a}_j + \frac{1}{2} \sum_{ijkl} \langle ij | kl \rangle \hat{a}_i^\dagger \hat{a}_j^\dagger \hat{a}_l \hat{a}_k. \quad (3)$$

Here \hat{a}_i^\dagger (\hat{a}_i) are fermionic creation (annihilation) operators, and

$$h_{ij} = \int \psi_i^*(\mathbf{x}) \left(-\frac{1}{2} \nabla_{\mathbf{r}}^2 - \sum_{\alpha} \frac{Z_{\alpha}}{|\mathbf{r} - \mathbf{R}_{\alpha}|} \right) \psi_j(\mathbf{x}) \, d\mathbf{x}, \quad (4)$$

$$\langle ij | kl \rangle = \int \psi_i^*(\mathbf{x}_1) \psi_j^*(\mathbf{x}_2) \frac{1}{r_{12}} \psi_k(\mathbf{x}_1) \psi_l(\mathbf{x}_2) \, d\mathbf{x}_1 d\mathbf{x}_2 \quad (5)$$

are one- and two-electrons integrals, respectively. $\{\psi_i(\mathbf{x})\}_{i=1}^{N_{\text{so}}}$ are the spin-orbitals, which depend on a joined (spatial plus spin) coordinate of an electron, $\mathbf{x} = (\mathbf{r}, \sigma)$,

and constitute a spin-orbital basis of the size N_{so} . Typically spin-orbitals are themselves constructed as linear expansions over an auxiliary basis set of atomic-centered functions known as atomic orbitals.

The size of the one-electron basis determines the size of the matrix representation of \hat{H}_e , which is $2^{N_{\text{so}}} \times 2^{N_{\text{so}}}$. Thus, the exact algebraic solution is possible for molecules containing only few atoms. Eigenvectors of an operator (3) are known as full configurational interaction (FCI) states. Corresponding eigen-energies are commonly used as benchmarks for any approximate methods as they can be only improved by enlarging the one-electron basis set.

Using one of the conventional fermion-to-qubit transformations, such as the Jordan–Wigner (JW)^{17,18} or Bravyi–Kitaev (BK),^{19–23} the second-quantized fermionic Hamiltonian (3) can be iso-spectrally transformed to a qubit form,

$$\hat{H} = \sum_I C_I \hat{T}_I, \quad (6)$$

where C_I are deduced from one- and two-electron integrals (h_{ij} and $\langle ij | kl \rangle$), and \hat{T}_I operators are products of several spin operators,

$$\hat{T}_I = \dots \hat{\sigma}_1^{(I)} \hat{\sigma}_0^{(I)}, \quad (7)$$

which we call “Pauli words” for brevity. Each of $\hat{\sigma}_i^{(I)}$, is one of the Pauli \hat{x}_i , \hat{y}_i , or \hat{z}_i operators.

B. Qubit coupled cluster method

The QCC method relies on a two-tier parametrization of a trial wave function: 1) the qubit mean-field (QMF) description^{24,25} and 2) multi-qubit transformations to account for electron correlation.¹³ The QMF part uses the simplest variational Ansatz that is possible on a quantum computer: a direct product of superposition states of individual qubits,

$$|\Omega\rangle = \prod_{i=1}^{N_q} |\Omega_i\rangle, \quad (8)$$

where

$$|\Omega_i\rangle = \cos\left(\frac{\theta_i}{2}\right) |\alpha\rangle + e^{i\phi_i} \sin\left(\frac{\theta_i}{2}\right) |\beta\rangle \quad (9)$$

is a so-called spin-coherent state for the i -th qubit.^{26–29} ϕ_i and θ_i are azimuthal and polar angles on the “Bloch sphere” of the i -th qubit, respectively, and $|\alpha\rangle$ and $|\beta\rangle$ are “up” and “down” eigenstates of the \hat{z}_i operator. The QMF ground-state energy is defined as a minimum of the corresponding energy functional with respect to all Bloch angles $\Omega = \{\phi_i, \theta_i\}_{i=1}^{N_q}$:

$$E_{\text{QMF}} = \min_{\Omega} \langle \Omega | \hat{H} | \Omega \rangle. \quad (10)$$

The energy functional (10) has an exceptionally simple form in terms of Bloch angles. To derive it, one needs to replace all Pauli operators in Eq. (6) with functions according to the rule

$$\begin{aligned}\hat{x}_i &\rightarrow \cos \phi_i \sin \theta_i, \\ \hat{y}_i &\rightarrow \sin \phi_i \sin \theta_i, \\ \hat{z}_i &\rightarrow \cos \theta_i\end{aligned}\quad (11)$$

and convert operator products to ordinary products of real numbers. The domain of definition for angles is

$$\phi_i \in [0, 2\pi), \quad (12)$$

$$\theta_i \in [0, \pi), \quad i = 1, \dots, N_q. \quad (13)$$

In what follows we consider the QMF energy function as a separate approximation to the solution of the electronic structure problem.

The second step in the QCC method introduces a multi-qubit unitary transformation

$$U(\boldsymbol{\tau}) = \prod_{k=1}^{N_{\text{ent}}} \exp(-i\tau_k \hat{P}_k/2), \quad (14)$$

where \hat{P}_k are the multi-qubit Pauli words (“entanglers”), which are responsible for multi-qubit entanglement, and τ_k are the corresponding amplitudes that are optimized within a domain

$$\tau_k \in [0, 2\pi), \quad k = 1, \dots, N_{\text{ent}}. \quad (15)$$

The total QCC energy assumes the form

$$E_{\text{QCC}} = \min_{\boldsymbol{\Omega}, \boldsymbol{\tau}} \langle \boldsymbol{\Omega} | U^\dagger(\boldsymbol{\tau}) \hat{H} U(\boldsymbol{\tau}) | \boldsymbol{\Omega} \rangle. \quad (16)$$

The transformed Hamiltonian $U^\dagger(\boldsymbol{\tau}) \hat{H} U(\boldsymbol{\tau})$ in Eq. (16) can be calculated recursively by the formula:¹³

$$\begin{aligned}\hat{A}^{(k)}(\tau_k, \dots, \tau_1) &= e^{i\tau_k \hat{P}_k/2} \hat{A}^{(k-1)}(\tau_{k-1}, \dots, \tau_1) e^{-i\tau_k \hat{P}_k/2} \\ &= \hat{A}^{(k-1)} - i \frac{\sin \tau_k}{2} [\hat{A}^{(k-1)}, \hat{P}_k] \\ &\quad + \frac{1}{2} (1 - \cos \tau_k) \hat{P}_k [\hat{A}^{(k-1)}, \hat{P}_k],\end{aligned}\quad (17)$$

where $k = 1, \dots, N_{\text{ent}}$ and $\hat{A}^{(0)} = \hat{H}$. This procedure produces $3^{N_{\text{ent}}}$ distinct operator terms, but frequently good results can be achieved already at small N_{ent} . The problem of optimal choice of entanglers is addressed in Ref. 13, and we assume here that it is already solved, so that Eq. (17) has been used N_{ent} times to generate a list of operators and trigonometric factors that depend on $\{\tau_k\}$. The final form of the QCC energy functional can now be obtained by applying the rule (11) to each of the operators in the list and summing them together. The resulting expression is a function of amplitudes $\boldsymbol{\tau}$ and angles $\boldsymbol{\Omega}$. Classical minimization of that function yields the QCC ground-state energy.

The QMF and QCC energy functions are sums of products, where each individual term consists of the factors $\sin(\phi_i)$, $\cos(\phi_i)$, $\sin(\theta_i)$, $\cos(\theta_i)$, $\sin(\tau_i)$, and $[1 - \cos(\tau_i)]$ that occur no more than once; in other words, they are polylinear functions of those factors. As our experience shows, the search for the global minimum of QMF or QCC energy starting from a random guess is a difficult task; the minimization procedure tends to converge to different local minima. The situation is very much like as in the conventional multiconfigurational self-consistent field (MCSCF) method:³⁰ the corresponding non-linear equations have multiple solutions. Note that such a problem is less common (albeit possible) in the single-configuration Hartree–Fock method: in the most of the implementations the Fock matrix and its eigenvalues—orbital energies—are available, and one can enforce the Aufbau principle by populating the orbitals with the lowest energies first,³¹ avoiding high-energy local minima that describe core-hole or highly excited Rydberg states. Unfortunately, this option is not available in the QMF method. Thus, a strategy how to maximize the likelihood of finding the global minimum is needed.

C. Domain reduction by folding

The difficulty in locating the global minimum in either QMF or QCC theories can be rationalized as follows: Despite the polylinear form of the energy functional, each trigonometric factor is a non-linear function with at least one extremum in the domain of definition; “individual” extrema multiply as the number of variables grows, and odds for locating the global minimum are greatly diminish.

As the local extrema of individual trigonometric factors are partially responsible for this problem, we confine them in reduced domains by creating multiple branches of the trigonometric functions with the aid of auxiliary discrete variables. We refer to this procedure as “folding” and illustrate it below for each class of continuous variables separately.

Consider $\{\theta_i\}$ variables first. In the domain of definition, Eq. (13), each $\sin(\theta_i)$ has a maximum at $\theta_i = \pi/2$ and is symmetric with respect to this line, while $\cos(\theta_i)$ are monotonic and anti-symmetric. If we reflect a piece of the cosine function on $[\pi/2, \pi]$ back to $[0, \pi/2)$, we obtain a second branch which is negation of the original cos function in the same range, see Fig. 1a. Both branches can be encoded in the reduced domain by new discrete variables Z_i as:

$$\begin{aligned}\sin \theta_i &\rightarrow \sin \theta_i, \\ \cos \theta_i &\rightarrow Z_i \cos \theta_i,\end{aligned}\quad (18)$$

where

$$\theta_i \in [0, \pi/2), \quad Z_i \in \{\pm 1\} \quad (19)$$

For $\{\phi_i\}$ angles we have the same trigonometric functions as for θ_i -s, but on the $[0, 2\pi)$ domain [see Eq. (12)].

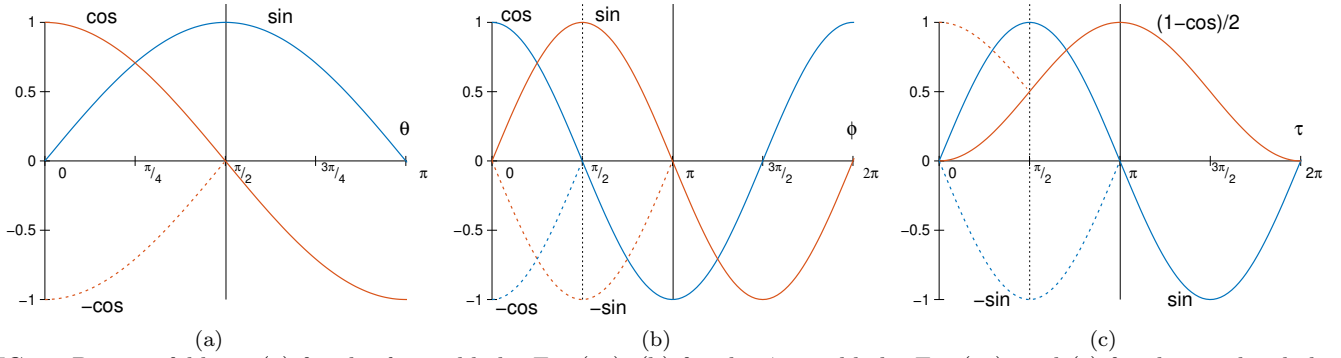


FIG. 1. Domain folding: (a) for the θ variable by Eq. (18), (b) for the ϕ variable by Eq. (21), and (c) for the amplitude by Eq. (25). New branches are dashed lines.

This suggests that the domain folding can be performed twice. Indeed, first we notice that $\cos(\phi)$ is even, while $\sin(\phi)$ is odd with respect to the line $\phi = \pi$, see Fig. 1b. Thus, introducing new discrete variables Q_i , we can write:

$$\begin{aligned} \sin \phi_i &\rightarrow Q_i \sin \phi_i, \\ \cos \phi_i &\rightarrow \cos \phi_i. \end{aligned} \quad (20)$$

In the new domain, $\phi_i \in [0, \pi)$, the cosine function is odd, but both branches of sin are even. Therefore, we can perform another folding by introducing new discrete variables W_i :

$$\begin{aligned} \sin \phi_i &\rightarrow Q_i \sin \phi_i, \\ \cos \phi_i &\rightarrow W_i \cos \phi_i, \end{aligned} \quad (21)$$

where

$$\phi_i \in [0, \pi/2), \quad Q_i, W_i \in \{\pm 1\}. \quad (22)$$

Amplitudes $\{\tau_i\}$ enter the QCC energy expression as $\sin(\tau_i)$ or $[1 - \cos(\tau_i)]$ functions (Fig. 1c). The domain folding can be performed twice: first, with respect to the line $\tau = \pi$, which maps $[1 - \cos(\tau)]$ to itself and creates two branches of $\sin(\tau)$,

$$\begin{aligned} \sin \tau_i &\rightarrow F_i \sin \tau_i, \\ [1 - \cos \tau_i] &\rightarrow [1 - \cos \tau_i], \end{aligned} \quad (23)$$

with

$$\tau_i \in [0, \pi), \quad F_i \in \{\pm 1\}, \quad (24)$$

and second, with respect to the line $\tau = \pi/2$, which creates additional branch for $[1 - \cos(\tau)]$:

$$\begin{aligned} \sin \tau_i &\rightarrow F_i \sin \tau_i, \\ [1 - \cos \tau_i] &\rightarrow [1 - G_i \cos \tau_i], \end{aligned} \quad (25)$$

with

$$\tau_i \in [0, \pi/2), \quad F_i, G_i \in \{\pm 1\}. \quad (26)$$

Note that after the foldings all branches of the trigonometric functions become monotonic. Minimization of the

QCC energy expression now requires continuous optimization over reduced domains plus discrete optimization over $\{Z_i, Q_i, W_i, F_i, G_i\}$ variables. This mixed discrete-continuous optimization is done in two alternating steps: 1) for fixed values of discrete variables the continuous variables are optimized, 2) for fixed values of the continuous variables the discrete variables are optimized. For efficient discrete optimization the folded QCC energy function is expressed in the generalized Ising form

$$\hat{H}_{\text{Is}}^{\text{gen}} = \sum_i A_i \hat{z}_i + \sum_{ij} B_{ij} \hat{z}_i \hat{z}_j + \sum_{ijk} C_{ijk} \hat{z}_i \hat{z}_j \hat{z}_k + \dots \quad (27)$$

where a single \hat{z}_i operator represents one of the discrete variables $\{Z_i, Q_i, W_i, F_i, G_i\}$, and coefficients A_i, B_{ij} , and C_{ijk} are derived from values of trigonometric factors with fixed continuous variables. Obtaining the lowest eigenstate of $\hat{H}_{\text{Is}}^{\text{gen}}$ is equivalent to the discrete optimization step.

D. Solving the generalized Ising Hamiltonians for various foldings

Multiple levels of folding have been introduced in Sec. II C: it is possible to fold once in θ_i and twice in ϕ_i and τ_i . While it is tempting to use the maximum possible folding, there is a trade-off between simplification of the energy landscape due to the domain reduction and the complexity of the resulting Ising Hamiltonians. Each level of folding³² introduces additional \hat{z}_i variables into Eq. (27). Unfortunately, practical quantum annealers, like the D-Wave 2000Q system, can *not* deal with the generalized form (27). To convert Eq. (27) to a 2-local form containing at most quadratic terms [Eq. (1)], one has to introduce auxiliary variables (e.g. $\hat{z}_{ij}^{(2)} = \hat{z}_i \hat{z}_j$) to lower the rank of high-order terms and the corresponding constraints to avoid spurious solutions. This step additionally increases the qubit count of the discrete optimization. Therefore, calculations done on D-Wave's 2000Q quantum annealer do not use the full folding scheme.

To assess capability of our folding technique in full, we simulate an idealized quantum annealer on a classical

computer by evaluating the ground state of a generalized Ising Hamiltonian (27) using a direct diagonalization in the full multi-qubit Hilbert space of the problem. Due to exponential growth of this space with the number of qubits we treat only relatively small systems by this “ideal Ising machine.”

We introduce the following notation to discuss performance of the folding procedure at intermediate levels:

$$(m, n), \text{ where } 1 \leq m \leq 3, 0 \leq n \leq 2. \quad (28)$$

m indicates how many times the folding was done in mean-field variables θ and ϕ , while n the number of foldings in τ . In particular, $m = 1$ means that the folding is done once in θ variable for each qubit by Eq. (18), while $m = 2, 3$ means that θ -folding is made once, but additionally, ϕ -foldings are made once or twice by Eqs. (20) or (21), respectively. Overall, this introduces N_q , $2N_q$, or $3N_q$ \hat{z}_i operators to the generalized Ising Hamiltonian (27) for $m = 1-3$. Additionally, since there are no amplitudes the QMF method, n values may be omitted to give a notation “ $(m,)$.”

For the QCC method single- [$n = 1$, Eq. (23)], double- [$n = 2$, Eq. (25)], as well as no-folding ($n = 0$) variants are possible. As a result, 0, N_{ent} , or $2N_{\text{ent}}$ new operators can be defined for $n = 0, 1$, and 2, respectively. Overall, there are $(mN_q + nN_{\text{ent}})$ \hat{z}_i operators at the folding level (m, n) .

III. NUMERICAL STUDIES

A. Preparatory calculations and optimization setup

We calculated potential energy curves using the QMF and QCC methods for the LiH and H₂O molecules, and the QMF method for C₆H₆ on both a classical computer and the D-Wave 2000Q system. Near equilibrium geometries the QCC method provides the chemical accuracy, $\leq 1 \text{ kcal mol}^{-1}$, within a chosen basis and active space. However, to make our examples more challenging, we consider a few molecular structures outside the equilibrium, namely: $R(\text{Li-H}) = 3.20 \text{ \AA}$ (the equilibrium value is *ca.* 1.54 \AA), the symmetrically stretched to $R(\text{O-H}) = 2.05 \text{ \AA}$ water molecule (the equilibrium value is *ca.* 0.96 \AA), and a symmetrically elongated benzene ring with $R(\text{C-C}) = 1.5914 \text{ \AA}$ (the equilibrium value is *ca.* 1.34 \AA), see Fig. 2. For more technical details on preparatory calculations see Table II.

The domain folding technique paired with a quantum annealer is assessed against a simple gradient-based local optimization (several popular local gradient-based continuous optimization algorithms are compared in Appendix B). Namely, starting from a random guess for Bloch angles and amplitudes and using a local optimization algorithm with and without annealing, we collect statistics how often each of the minima has been reached out of 100 runs.

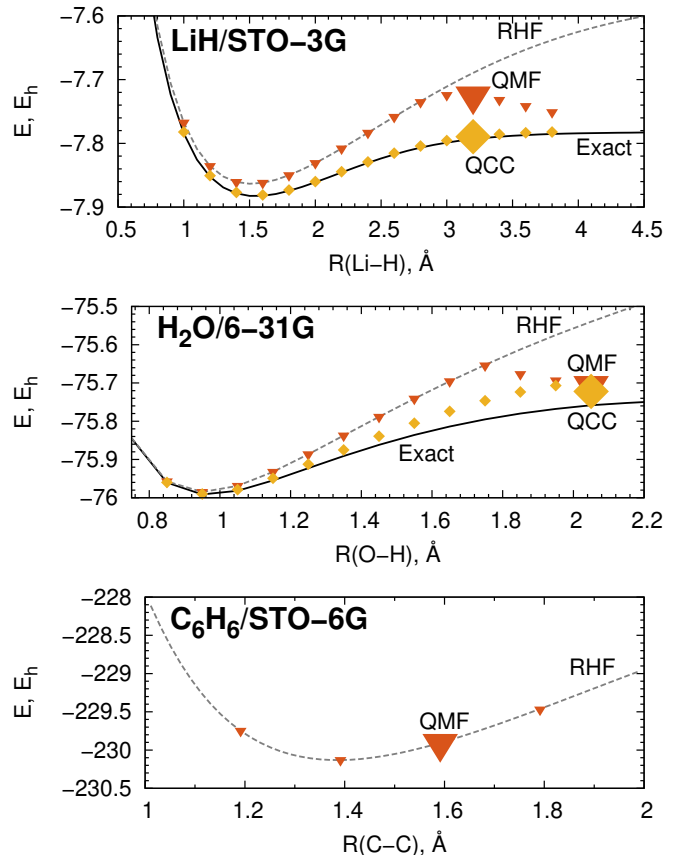


FIG. 2. Potential energy surface cuts for all molecules considered in the study. Restricted Hartree-Fock (RHF) and exact, complete active space configurational interaction (CASCI), curves were calculated on a classical computer using the GAMESS quantum chemistry package.³³ Magnified symbols correspond to molecular configurations for which the domain folding plus annealing assessment is done.

Generalized Ising Hamiltonians for different folding levels were generated as described in Sec. II D. Annealing is done on the ideal Ising machine and the D-Wave 2000Q system, but for the latter the corresponding generalized Ising Hamiltonians were converted to a 2-local Ising form (1) with the aid of D-Wave’s Ocean software.³⁴ Biases (h_i) and coupling terms (J_{ij}) of the Ising Hamiltonian (1) were computed on a classical computer; the resulting Hamiltonians were embedded onto D-Wave’s 2000Q using the minor-miner algorithm³⁵ using a cutoff of 1×10^{-2} . Qubit counts for each embedding are reported in Table I. A constant annealing time of $100 \mu\text{s}$ was used for all molecules, and the number of samples was equal to 1000. Bloch angles and amplitudes were updated using L-BFGS-B gradient optimization algorithm based on the minimum energy sampled from the annealer.

TABLE I. The number of qubits used by D-Wave’s 2000Q system to represent a QMF/QCC problem for a given molecule. Ranges reflect variation of this count due to neglecting the small terms in parametrized Ising Hamiltonians uploaded onto the annealer.

| Molecule | Qubit count in the Ising form | |
|-------------------------------|-------------------------------|---------------|
| | (1,0) folding | (1,1) folding |
| LiH | 9–14 | 28–35 |
| H ₂ O | 14–22 | 128–136 |
| C ₆ H ₆ | 800–900 ^a | – |

^a Only QMF simulations were performed, so that in the absence of amplitudes the folding scheme is (1,).

B. QMF and QCC simulations for LiH

A stretched LiH molecule is an example of a spin-broken system. Although the molecular orbitals that have been used to generate the qubit Hamiltonian (6) were taken from the restricted Hartree–Fock (RHF) calculations, the intrinsic ability of the QMF method to break symmetry²⁴ lead to the solution that was not a pure singlet, much like as in the *unrestricted* Hartree–Fock method, see Fig. 2. In such a situation one would expect a competition between several low-lying symmetry-broken solutions which are characterized by markedly different values of Bloch angles. Indeed, even in the QMF method without the domain folding there are several low-lying local minima, which lower a chance to reach the ground state as can be seen in Fig. 3a. Successive domain foldings in Bloch angles eliminate chances to converge to anything but the true ground state almost entirely. Thus, the domain folding technique greatly enhances probability to reach the true minimum even in a presence of symmetry breaking. It must be noted that symmetry breaking does not necessarily imply incorrect calculations; instead, such a phenomenon indicates existence of a complicated open-shell ground state in molecules with partly ruptured bonds or containing transition metal atoms.

Introducing electron correlation at the QCC level does change statistics, but not the physics. For highly stretched molecules the primary role of electron correlation is symmetry restoration *via* proper mixing of open-shell atomic states that emerge in a course of dissociation. Since symmetry constraints are quite rigid, we do not expect multiple low-lying minima. Indeed, QCC calculations bring the total energy to be within 2 kcal mol⁻¹ from exact, but the main effect of amplitude folding is already seen at the (1, 1) level, see Fig. 3b. While for the unfolded problem the probability of finding the true ground state is merely 20 %, it raises to almost 60 % and, finally, to more than 85 % by going to (1, 1) and (3, 1) levels, respectively. It is also clear that the Bloch angle foldings are more important than the amplitude foldings, as it should be for the symmetry-controlled case: moving to the highest (3, 2) level, *i.e.* simplifying the amplitude optimization even more, does not improve the probability to reach the ground state.

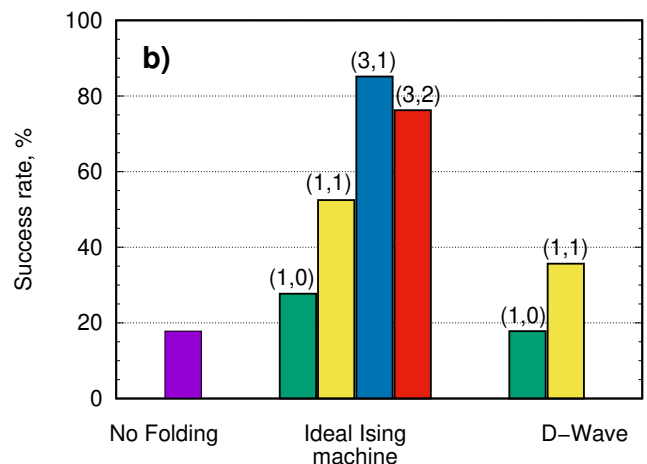
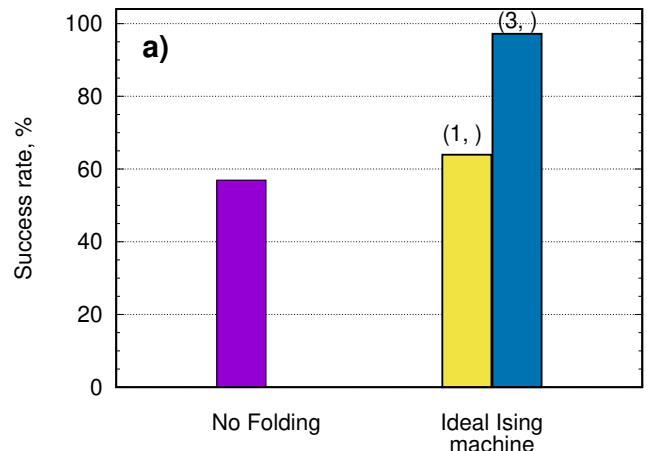


FIG. 3. Global minimum search success rate for the QMF (a) and QCC (b) calculations of the stretched LiH molecule. Different folding levels are labelled according to Sec. IID.

Fig. 3b also assesses the performance of the domain folding technique on the D-Wave 2000Q system. It is clear that the D-Wave 2000Q annealer, similar to the ideal Ising machine, systematically improves the chance to reach the ground state as the level of folding increases. There is still a minor gap in efficiency between the real annealer and an idealized device; we comment on the possible reasons more in Sec. III C.

C. QCC simulations for H₂O

A symmetric stretch of the H₂O molecule is the classical test for methods aimed at treating the strong correlation problem.³⁶ The most difficult situation, however, is not when bonds are completely broken but rather when they are “half-broken”. In such a nuclear configuration atomic states are heavily mixed with relative weights that are controlled not only by symmetry but also the interaction strength.

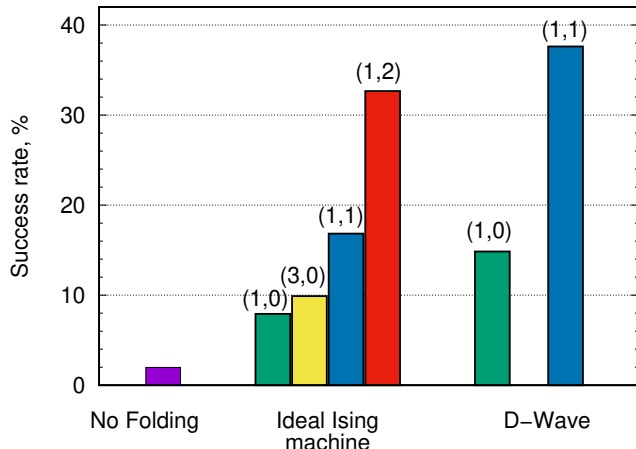


FIG. 4. Global minimum search success rate for the QCC calculations of the stretched H_2O molecule.

As evident from Fig. 4, the QCC optimization problem is extremely difficult: the probability to find the ground state without folding is just a few percent—one needs several dozens of tries to reach the ground state once! Various folding schemes shown in Fig. 4 do improve the situation, albeit to a different extent. Contrary to the LiH case, Bloch-angle foldings help only moderately, increasing the chance to reach the ground state to $\sim 10\%$ at the (3,0) level. This essentially means that the correlated solution is of the same symmetry as the mean-field one, and the mean-field solution is not symmetry-broken. This is additionally corroborated by the fact that even a single amplitude folding raises the chance to reach the ground state to 17%, which is a substantial improvement over the unfolded result and any of the Bloch-folded counterparts. Finally, (1,2) folding brings the chance to 33%: now one needs only 3 runs on average to reach the ground state.

To our surprise, the D-Wave 2000Q system performs *better* than an ideal Ising machine, as can be seen from Fig. 4. There are several plausible explanations of this phenomenon: different efficiency of local optimization methods (method of moving asymptotes (MMA) on the idealized Ising machine *vs.* L-BFGS-B for the D-Wave 2000Q system, see Appendix B) or smoothing of the energy landscape on the D-Wave system because of neglecting small terms in Ising Hamiltonians, so that the shallow minima are missed. We ruled out the smoothing as a reason: implementing similar strategy on the ideal Ising machine shown that the statistics is either almost unaffected (for small cutoffs) or so strongly skewed that is clearly incorrect. Thus, it is likely that slight variations of the efficiency of optimization algorithms plus statistical fluctuations may explain the difference. However, these variations do not affect the main conclusion: the domain folding provides *systematic* improvement of the global search.

D. QMF simulations for C_6H_6

Our final example is large-scale, 36-qubit, QMF calculations of a slightly expanded C_6H_6 ring. In this case it is not possible to simulate the problem on an ideal Ising machine due to excessive memory requirements.

Results show that a single θ folding drastically increases chances to obtain the global minimum of energy: from less than 5% to 40%. It might be somewhat surprising that QMF calculations without the folding face so profound difficulties in reaching the true minimum near the equilibrium geometry, where a single-determinant solution is stable to any kind of symmetry breaking. Moreover, such calculations have to be equivalent to the RHF ones (see Fig. 2), which can be performed with ease on a classical computer. The resolution of this apparent paradox lies in the fact that, as was already noted at the end of Sec. II B, the QMF method has no access to quantities like orbital energies and, has to search through multiple orbital population patterns to find the lowest-energy one. At the same time, in the RHF method with the Fock matrix diagonalization, the Aufbau principle³¹ immediately rules out the majority of high-energy minima.

We provide in-depth analysis of the problem in Appendix C; here we only emphasize that a single domain folding in θ_i variables plus quantum annealing can be perceived as a substitute of the Aufbau principle for the QMF method.

IV. CONCLUSIONS

We have presented and assessed the domain folding technique that allows one to exploit optimization capacity of quantum annealers in quantum chemistry calculations. The domain folding uses multiple local symmetries that present in the qubit mean-field (QMF) and qubit coupled cluster (QCC) methods—which were originally formulated for use on universal quantum computers—to greatly enhance chances to reach the global minimum of electronic energy. On the set of electronic structure calculations for LiH, H_2O , and C_6H_6 molecules we have demonstrated the advantages of the domain folding both on the ideal Ising machine and on the D-Wave 2000Q system.

Although preparatory stages for QMF/QCC calculations require substantial classical precomputations, the use of annealers makes the QMF and QCC methods quite promising in situations with symmetry breaking/strong correlation, in which multiple solutions of the electronic structure problem exist.³⁰ To the best of our knowledge, the satisfactory treatment for such cases were not available before, but with the domain folding technique coupled to quantum annealers, they can be treated much better.

Additionally, we found (see Sec. III D) that any variational qubit Ansatz, as a global minimization problem, would experience difficulties in locating the global minimum (even in the simplest parametrization, like our QMF form), due to an exponential number of energy minima.

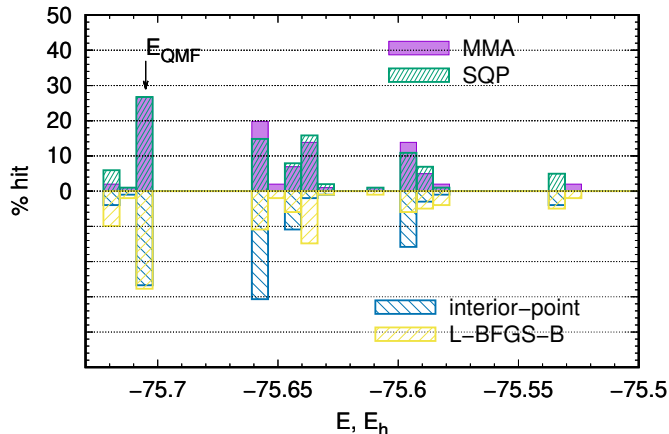


FIG. 5. Stationary point location statistics for different local optimization algorithms in the QCC method for the H_2O molecule. A half of the results are mirrored to improve readability. Acronyms are explained in Appendix B.

Recently, such difficulties have been reported for another VQE approach in Ref. 37. The domain folding technique mitigates the problem, and for the case of QMF can be thought of as a substitute for the missing Aufbau principle, see Appendix C. Moreover, the domain folding technique for the QCC method, which goes beyond the mean-field treatment, may open opportunities to study strongly correlated systems.

ACKNOWLEDGMENTS

A.F.I. acknowledges financial support from the Natural Sciences and Engineering Research Council of Canada.

Appendix A: Preparatory calculations

Essential details on preparatory calculations are given in Table II.

Appendix B: Comparison of different continuous optimization methods

We tested several local continuous optimization methods on a single problem of QCC energy optimization for the H_2O molecule to confirm that neither of them is superior to others in global search. These methods are:

1. The method of moving asymptotes (MMA)⁴⁰ as implemented in Ref. 41 available through the `NLOpt.jl` Julia⁴² package. It is a globally convergent method, which is especially convenient when function/gradient evaluations are very time-consuming, which is the case for an idealized Ising machine.

2. The L-BFGS-B method^{43,44} available through Python API on D-Wave’s system. It is less robust than MMA, but the cost of discrete energy minimization is determined by the D-Wave 2000Q system.

- 3–4. The sequential quadratic programming (SQP)⁴⁵ and interior-point^{46–48} methods from the MATLAB⁴⁹ suit. These methods were not used in calculations with the domain folding, rather, they are included as references to the readily available algorithms that may be chosen to solve QMF or QCC problems on a classical computer.

Assessment of different continuous optimizers in the case of the H_2O molecule is presented in Fig. 5. Clearly all methods are quite comparable in their ability to find various local minima in the system, and for all of them finding the global minimum is indeed a difficult task. It is interesting, that less robust methods, such as L-BFGS-B and interior-point ones, are slightly more efficient in the global search problem. It is likely that these methods may simply miss some of the high-energy shallow minima, thus improving the statistics for deeper minima including the ground state.

Appendix C: On the equivalence of QMF and restricted Hartree–Fock (RHF) calculations

For many molecules, especially near their equilibrium configurations, the RHF single-determinant wave function is a qualitatively correct representation of the exact one; it is stable with respect all possible spin and electron-number variations. The QMF calculations that start from the fermionic Hamiltonian (3) written in the basis of the canonical Hartree–Fock orbitals have to converge to the RHF energy.²⁵ However, the pristine QMF energy minimization has non-negligible probability to converge to other, higher-energy solutions, as evident from Fig. 3a and results of Sec. III D. Here we investigate this QMF deficiency, provide the reasoning why the RHF method is largely immune to it, and find out why the domain folding in θ_i variables plus quantum annealing can be perceived as a cure.

First, we observe that a single-determinant wave function $|\Phi\rangle$ can be characterized not only by the total number of electrons, N_e , but also the orbital population vector, in which every orbital is either populated (1) or not (0), according to the mean values of orbital population operators

$$\hat{n}_i = a_i^\dagger a_i, \quad i = 1, \dots, N_{\text{so}}, \quad (\text{C1})$$

$$\langle \hat{n}_i \rangle = \langle \Phi | \hat{n}_i | \Phi \rangle = \{0, 1\}. \quad (\text{C2})$$

After any of the fermion-to-qubit transformations, the operators (C1) acquire the Ising form:²⁰

$$\hat{n}_i \rightarrow \hat{n}_i(\hat{z}_i). \quad (\text{C3})$$

TABLE II. Fermionic and qubit Hamiltonians construction parameters for molecules used in the work. Canonical set of the Hartree–Fock molecular orbitals is used throughout.

| Property | Molecule | | |
|--|--|---|--|
| | LiH ^a | H ₂ O ^a | C ₆ H ₆ |
| Molecular configuration | $R(\text{Li-H}) = 3.20 \text{ \AA}$ | $R(\text{O-H}) = 2.05 \text{ \AA}$ $\angle\text{HOH} = 107.6^\circ$ | $R(\text{C-C}) = 1.5914 \text{ \AA}$ $R(\text{C-H}) = 1.0802 \text{ \AA}$ |
| Atomic basis set ^b | STO-3G | 6-31G | STO-6G |
| Total number of molecular orbitals | 6 | 13 | 36 |
| Number of spin-orbitals in active space, N_{so} | 6 | 8 | 36 |
| Number of electrons in active space | 2 | 4 | 18 |
| Fock space dimension, $2^{N_{\text{so}}}$ | 64 | 256 | 6.87×10^{10} |
| Fermion-to-qubit mapping | parity ^c | Bravyi–Kitaev (BK) | Bravyi–Kitaev (BK) |
| Qubit count, N_q | 4 ^d | 6 ^d | 36 |
| Entanglers for QCC, \hat{P}_i | $\hat{x}_2\hat{y}_0, \hat{x}_3\hat{x}_2\hat{x}_1\hat{y}_0, \hat{y}_3\hat{x}_2\hat{y}_1\hat{y}_0$ | $\hat{P}, \hat{z}_5\hat{z}_2\hat{P}, \hat{x}_5\hat{x}_2\hat{P}$ $\hat{x}_2\hat{y}_0, \hat{y}_5\hat{x}_3, \hat{x}_4\hat{y}_1$ $\hat{P} = \hat{x}_4\hat{x}_3\hat{x}_1\hat{y}_0$ | – |

^a More details on the electronic structure calculations and qubit mean-field (QMF)/QCC setup can be found in Ref. 13.

^b From the Basis Set Exchange library.³⁸

^c Described in Ref. 39.

^d Qubit parity symmetries have been used to reduce the qubit count by 2 as compared to N_{so} .

In turn, Eq. (C3) becomes a function of only $\cos(\theta_i)$ after application of Eq. (11). A simple observation shows that the integer values in Eq. (C2) are, in general, compatible with only $\theta_i = 0$ or π , when $\cos\theta_i = \pm 1$. This essentially means that the RHF solution is characterized by *fixed* θ_i angles either 0 or π ; which, in turn, implies that continuous optimization of θ_i is not necessary. Moreover, as follows from Eq. (9), for $\theta_i = 0$ or π the wave function does not depend (apart from an irrelevant global phase) on ϕ angles too. Thus, the QMF energy optimization is reduced to the discrete part only. However, without the annealing it is still exponentially hard, which explains why the QMF method has difficulties in locating the global minimum.

It must be noted that such a problem does not impact strongly common implementations of the RHF method on a classical computer. Most of the computational schemes

repeatedly construct and diagonalize the Fock matrix, which gives access to orbital energy estimates. The latter can be sorted, and only lowest $2N_e$ of them (“the Aufbau principle”) can be used to built the ground electronic wave function. In general, for a typical molecular system without stretched bonds or transition-metal ions, only a small fraction of orbitals have energies close to the Fermi level and can be potentially swapped during the self-consistent cycle, which translates into the small number of potential candidates for the global minimum. In the opposite case, however, when many orbitals are in energy proximity to the Fermi level, the traditional Hartree–Fock algorithms may experience difficulties in locating the lowest-energy solution. In such situations the QMF method with domain folding and quantum annealing may become the method of choice, as it can deal with the plethora of local minima efficiently.

* ilya.ryabinkin@otilumionics.com

¹ R. P. Feynman, *Int. J. Theor. Phys.* **21**, 467 (1982).

² M. W. Johnson, M. H. S. Amin, S. Gildert, T. Lanting, F. Hamze, N. Dickson, R. Harris, A. J. Berkley, J. Johansson, P. Bunyk, E. M. Chapple, C. Enderud, J. P. Hilton, K. Karimi, E. Ladizinsky, N. Ladizinsky, T. Oh, I. Perminov, C. Rich, M. C. Thom, E. Tolkacheva, C. J. S. Truncik, S. Uchaikin, J. Wang, B. Wilson, and G. Rose, *Nature* **473**, 194 (2011).

³ S. Boixo, T. F. Rønnow, S. V. Isakov, Z. Wang, D. Wecker, D. A. Lidar, J. M. Martinis, and M. Troyer, *Nat. Phys.* **10**, 218 (2014).

⁴ W. Lechner, P. Hauke, and P. Zoller, *Sci. Adv.* **1**, e1500838 (2015).

⁵ T. Inagaki, Y. Haribara, K. Igarashi, T. Sonobe, S. Tamate, T. Honjo, A. Marandi, P. L. McMahon, T. Umeki, K. Enbutsu, O. Tadanaga, H. Takenouchi, K. Aihara, K.-I.

Kawarabayashi, K. Inoue, S. Utsunomiya, and H. Takesue, *Science* **354**, 603 (2016).

⁶ P. L. McMahon, A. Marandi, Y. Haribara, R. Hamerly, C. Langrock, S. Tamate, T. Inagaki, H. Takesue, S. Utsunomiya, K. Aihara, R. L. Byer, M. M. Fejer, H. Mabuchi, and Y. Yamamoto, *Science* **354**, 614 (2016).

⁷ T. Inagaki, K. Inaba, R. Hamerly, K. Inoue, Y. Yamamoto, and H. Takesue, *Nat. Photonics* **10**, 415 (2016).

⁸ T. Kadowaki and H. Nishimori, *Phys. Rev. E* **58**, 5355 (1998).

⁹ G. E. Santoro, R. Martoňák, E. Tosatti, and R. Car, *Science* **295**, 2427 (2002).

¹⁰ D. A. Battaglia, G. E. Santoro, and E. Tosatti, *Phys. Rev. E* **71**, 066707 (2005).

¹¹ R. Xia, T. Bian, and S. Kais, *J. Phys. Chem. B* **122**, 3384 (2018).

¹² M. Streif, F. Neukart, and M. Leib, arXiv e-prints (2018),

- arXiv:1811.05256 [quant-ph].
- 13 I. G. Ryabinkin, T.-C. Yen, S. N. Genin, and A. F. Izmaylov, *J. Chem. Theory Comput.* **14**, 6317 (2018), arXiv:1809.03827 [quant-ph].
 - 14 A. Peruzzo, J. McClean, P. Shadbolt, M.-H. Yung, X.-Q. Zhou, P. J. Love, A. Aspuru-Guzik, and J. L. O’Brien, *Nat. Commun.* **5**, 4213 (2014).
 - 15 D. Wecker, M. B. Hastings, and M. Troyer, *Phys. Rev. A* **92**, 042303 (2015).
 - 16 “D-Wave announces D-Wave 2000Q Quantum Computer and first system order,” D-Wave Systems Inc. press release (2017), <https://www.dwavesys.com/press-releases/d-wave%20announces%20A0d-wave-2000q-quantum-computer>.
 - 17 P. Jordan and E. Wigner, *Z. Phys.* **47**, 631 (1928).
 - 18 A. Aspuru-Guzik, A. D. Dutoi, P. J. Love, and M. Head-Gordon, *Science* **309**, 1704 (2005).
 - 19 S. B. Bravyi and A. Y. Kitaev, *Ann. Phys.* **298**, 210 (2002).
 - 20 J. T. Seeley, M. J. Richard, and P. J. Love, *J. Chem. Phys.* **137**, 224109 (2012).
 - 21 A. Tranter, S. Sofia, J. Seeley, M. Kaicher, J. McClean, R. Babbush, P. V. Coveney, F. Mintert, F. Wilhelm, and P. J. Love, *Int. J. Quantum Chem.* **115**, 1431 (2015).
 - 22 K. Setia and J. D. Whitfield, ArXiv e-prints (2017), arXiv:1712.00446 [quant-ph].
 - 23 V. Havlíček, M. Troyer, and J. D. Whitfield, *Phys. Rev. A* **95**, 032332 (2017).
 - 24 I. G. Ryabinkin, S. N. Genin, and A. F. Izmaylov, *J. Chem. Theory Comput.* **15**, 249 (2019), arXiv:1806.00461 [physics.chem-ph].
 - 25 I. G. Ryabinkin, S. N. Genin, and A. F. Izmaylov, *J. Chem. Phys.* **149**, 214105 (2018), arXiv:1806.00514 [physics.chem-ph].
 - 26 J. M. Radcliffe, *J. Phys. A* **4**, 313 (1971).
 - 27 F. T. Arecchi, E. Courtens, R. Gilmore, and H. Thomas, *Phys. Rev. A* **6**, 2211 (1972).
 - 28 A. Perelomov, *Generalized Coherent States and Their Applications*, Theoretical and Mathematical Physics (Springer Science & Business Media, 2012).
 - 29 E. H. Lieb, *Commun. Math. Phys.* **31**, 327 (1973).
 - 30 C. Angeli, C. J. Calzado, R. Cimiraglia, S. Evangelisti, and D. Mayna, *Mol. Phys.* **101**, 1937 (2003).
 - 31 V. R. Saunders and I. H. Hillier, *Int. J. Quantum Chem.* **7**, 699 (1973).
 - 32 The folding introduced by Eq. (25) is special: each of $(1 - \cos \tau_i)$ factors gives rise to *two* new terms, one of those is dependent of G_i while the other is not. Overall, this leads to a $2^{N_{\text{ent}}}$ -fold increase in the number of terms of the resulting Ising Hamiltonian. This increase, however, is moderate as compared to the size of the entire QCC Ansatz ($3^{N_{\text{ent}}}$). On the other hand, a somewhat unexpected consequence of this additional expansion is: even at $\tau = 0$ there are *multiple* energy operators—one of those is the original \hat{H} , but others have the form

$$\hat{P}_k \cdots \hat{P}_1 \hat{H} \hat{P}_1 \cdots \hat{P}_k, \quad k = 1, \dots, N_{\text{ent}}.$$
 They appear each time when one of $G_i = -1$. It is not clear, however, if any lower than the QMF energy values may come from these expressions—we left this question open for future studies.
 - 33 M. S. Gordon and M. W. Schmidt, in *Theory and Applications of Computational Chemistry. The first forty years*, edited by C. E. Dykstra, G. Frenking, K. S. Kim, and G. E. Scuseria (Elsevier, Amsterdam, 2005) pp. 1167–1189, version from May 2013.
 - 34 “D-Wave’s Ocean tools,” <https://github.com/dwavesystems/dwave-ocean-sdk>, release 1.0.4.
 - 35 J. Cai, W. G. Macready, and A. Roy, arXiv e-prints (2014), <https://github.com/dwavesystems/minorminer>, arXiv:1406.2741 [quant-ph].
 - 36 M. L. Abrams and D. C. Sherrill, *Chem. Phys. Lett.* **404**, 284 (2005).
 - 37 J. Lee, W. J. Huggins, M. Head-Gordon, and K. B. Whaley, *J. Chem. Theory Comput.* **15**, 311 (2019).
 - 38 K. L. Schuchardt, B. T. Didier, T. Elsethagen, L. Sun, V. Gurumoorthi, J. Chase, J. Li, and T. Windus, *J. Chem. Inf. Model.* **47**, 1045 (2007).
 - 39 M. A. Nielsen, School of Physical Sciences The University of Queensland (2005).
 - 40 K. Svanberg, *SIAM J. Optimiz.* **12**, 555 (2002).
 - 41 S. G. Johnson, *The NLOpt nonlinear-optimization package* (2011).
 - 42 J. Bezanson, A. Edelman, S. Karpinski, and V. Shah, *SIAM Rev.* **59**, 65 (2017).
 - 43 R. Byrd, P. Lu, J. Nocedal, and C. Zhu, *SIAM J. Sci. Comput.* **16**, 1190 (1995).
 - 44 C. Zhu, R. H. Byrd, P. Lu, and J. Nocedal, *ACM Trans. Math. Softw.* **23**, 550 (1997).
 - 45 J. Nocedal and S. J. Wright, “Numerical optimization,” (Springer New York, 2006) Chap. 17, 2nd ed.
 - 46 R. Byrd, M. Hribar, and J. Nocedal, *SIAM J. Optimiz.* **9**, 877 (1999).
 - 47 R. H. Byrd, J. C. Gilbert, and J. Nocedal, *Math. Program.* **89**, 149 (2000).
 - 48 R. Waltz, J. Morales, J. Nocedal, and D. Orban, *Mathematical Programming* **107**, 391 (2006).
 - 49 MATLAB, *version R2018a Update 6 (9.4.0.949201)* (The MathWorks Inc., Natick, Massachusetts, 2018).